GEOCHEMISTRY

Volcanic origin for Younger Dryas geochemical anomalies ca. 12,900 cal B.P.

N. Sun[1], A. D. Brandon[1]*, S. L. Forman[2], M. R. Waters[3], K. S. Befus[2]

The Younger Dryas (YD) abrupt cooling event ca. 12.9 ± 0.1 ka is associated with substantial meltwater input into the North Atlantic Ocean, reversing deglacial warming. One controversial and prevailing hypothesis is that a bolide impact or airburst is responsible for these environmental changes. Here, highly siderophile element (HSE; Os, Ir, Ru, Pt, Pd, and Re) abundances and $^{187}Os/^{188}Os$ ratios were obtained in a well-dated sediment section at Hall's Cave, TX, USA to test this hypothesis. In Hall's Cave, layers below, above, and in the YD have $^{187}Os/^{188}Os$ ratios consistent with incorporation of extraterrestrial or mantle-derived material. The HSE abundances indicate that these layers contain volcanic gas aerosols and not extraterrestrial materials. The most likely explanation is that episodic, distant volcanic emissions were deposited in Hall's Cave sediments. Coupled $^{187}Os/^{188}Os$ ratios and HSE concentration data at close stratigraphic intervals are required to effectively differentiate between bolide and volcanic origins.

INTRODUCTION

The Younger Dryas (YD) event occurred from 12.9 to 11.7 thousand years (ka) in the Northern Hemisphere with abrupt cooling over a time interval of decades with temperatures possibly reaching 15°C colder than present (*1*, *2*). This cooling part of succession of climate variability in the Late Pleistocene resulted in progressive megafauna extinction (*3*). There are currently four hypotheses for the origins of the YD event. The prevailing hypothesis is that the cooling and stratification of the North Atlantic Ocean were a consequence of massive ice sheet discharge of meltwater and icebergs and resulted in reduction or cessation of the North Atlantic Conveyor. This is thought to be augmented by climate forcing with expanded snow cover in the Northern Hemisphere (*4*). Another persistent hypothesis is that global cooling was trigged by a bolide impact or airbursts (*1*). Stratigraphic markers supporting the YD impact hypothesis include elevated concentrations of carbon spherules, magnetic grains, nanodiamonds, and Pt and Ir abundance anomalies (*5*). These markers are found singularly or more at various sites globally and appear to reach peak abundances near or at the YD basal boundary layer. A meteorite crater potentially associated with the YD was recently found in Greenland, although not well dated (*6*).

A third hypothesis proposes that a supernova explosion in the Vela constellation could have depleted the ozone layer, resulting in greater ultraviolet exposure and atmospheric and surface changes that led to cooling (*7*). Last, a megaeruption of the Laacher See volcano ejected 6.3 km^3 [dense rock equivalent (DRE)] of zoned sulfur-rich phonolite magma far into the stratosphere at the time of the onset of the YD event (*8*). Volcanic aerosols and cryptotephra were dispersed throughout the Northern Hemisphere over a period of 2 months and affected the atmospheric optical density for over 1 year (*9*). Laacher See released a minimum of 2 metric megatons (Mt) of sulfur (possibly ranging up to 150 Mt) and is suggested to have triggered the sudden lowering of temperature coincident with YD climate change in the Northern Hemisphere (*10*).

Each of these four possible triggers for the YD event is complex, and there is not a clear consensus as to which mechanism or combination of these events initiated the YD cold period. Of these explanations, the impact hypothesis has received the most attention, but problems plague this hypothesis. The fundamental issue is delineating if the markers used to support the hypothesis extracted from the YD layers at various sites are really impact markers (*1*, *11*). The grains interpreted as carbon spherules and "elongates" and "glass-like carbon" have been instead identified as fungal sclerotia common in Northern Hemisphere forest litter and soils (*12*). In addition, the micrograins interpreted as hexagonal nanodiamonds from YD sites of Murray Springs (AZ) and Arlington Canyon on Santa Rosa Island (CA) are instead assessed as graphene/graphene aggregates (*13*). These disagreements are compounded by a lack of valid age control at many of the YD boundary (YDB) layer sites. It is now thought that only 3 of the 29 sites dated to the onset of YD event were within the prerequisite time period. Furthermore, there are problems in that the reproducibility of observations at the YD level has been questioned for the presence of magnetic grains, spherules, and Ir enrichments. Surovell *et al.* (*14*) failed to duplicate the magnetic grain or microspherule peaks associated with the YD basal boundary. Thus, there is a lack of consensus on how to interpret the impact markers.

Highly elevated concentrations of Ir together with enrichments of other highly siderophile elements (HSEs) (Os, Ir, Ru, Pt, Pd, and Re) in nearly chondritic ratios are considered indicators of a meteoritic contribution delivered when an extraterrestrial (ET) object affects the Earth or airbursts over it (*15*). These HSE enrichments may be from an external source because the Earth's crust has <0.1% of CI chondritic abundances (*16*). In addition, chondrites have $^{187}Os/^{188}Os$ ratios of around 0.125 (*17*), whereas continental crust has $^{187}Os/^{188}Os$ ratios of >1 (*18*), such that small amounts of ET material added to continental crust will shift the $^{187}Os/^{188}Os$ ratios of the hybridized material to lower values.

The cause of the elevated HSE concentrations and the Os isotopic ratios in YD layer sediments remains equivocal and has been used to both support and negate the YD impact hypothesis. For example, Petaev *et al.* (*19*) found a Pt enrichment accompanied with an

[1]Department of Earth and Atmospheric Sciences, University of Houston, Houston, TX 77004, USA. [2]Department of Geosciences, Baylor University, Waco, TX 76798, USA. [3]Center for the Study of the First Americans, Department of Anthropology, Texas A&M University, College Station, TX 77843, USA.
*Corresponding author. Email: abrandon@central.uh.edu

extremely high Pt/Ir but Al-poor signature in the Greenland Ice Sheet Project 2 ice core at the Bølling-Allerød/YD transition period, which they interpreted to be consistent with an ET impactor. Also, the elevated Pt abundance anomalies of 100 to 65,600 parts per trillion (ppt) at the onset of the YD in sites from North America is purportedly consistent with the Greenland ice core Pt data (*20*). Moore *et al.* (*9*) found Pt and Pd/Pt anomalies in the YD basal layer in South Carolina. These data are used to support a model of wide-ranged atmospheric input of platinum-rich dust during the YD, potentially related to a bolide impact or airburst. In contrast, the $^{187}Os/^{188}Os$ ratios obtained on YD basal boundary layers from widely dispersed locales in North America and Europe have largely been similar to those for continental crust or seawater with no evidence of unradiogenic $^{187}Os/^{188}Os$ ratios from ET or mantle sources, both having $^{187}Os/^{188}Os$ ratios of 0.11 to 0.13 (*21*, *22*). This is exceptional because <1% of ET material from an impactor mixed into continental crust would shift the resultant hybridized material away from terrestrial crustal $^{187}Os/^{188}Os$ values toward the less radiogenic values of $^{187}Os/^{188}Os$ chondrites (*17*). Only one site has been identified with an unradiogenic Os signature, with an $^{187}Os/^{188}Os$ ratio of 0.4 for the YD basal boundary layer at Melrose, PA (*22*). This signature is attributed to surface films on glass spherules with highly elevated Os concentrations and unradiogenic $^{187}Os/^{188}Os$ ratios of 0.113 to 0.121 that may have been caused by mobilization of Os within a bolide fireball and possibly terrestrial in origin and ejected as molten material following impact (*22*). An important question remains: Why are low $^{187}Os/^{188}Os$ ratios found only at one site and not more widely dispersed if it is derived from impact or air burst of a bolide?

The above studies show that there is no clear consensus on the interpretation of HSE concentrations and $^{187}Os/^{188}Os$ compositions of YD basal boundary sediments (*21*, *22*). A better understanding of their systematics is crucial for determining the role, if any, of a bolide event for the YD cooling and to refine conclusive evidence in the rock record for bolide impacts. To further examine this issue, we measured HSE abundances and $^{187}Os/^{188}Os$ isotope ratios in samples from Hall's Cave, TX, including those from the YDB. Hall's Cave formed in the Segovia Formation of the lower Cretaceous Edwards Group and contains sediments dating from 20,000 years before the present (B.P.) to present (*23*). The cave has a consistent depositional environment with minimal reworking or disturbance over this time period (*23*). The stratigraphy is well dated based on 162 accelerator mass spectrometry (AMS) ^{14}C dates from vertebrate fossils, snails, charcoal, and sediment chemical fractions (*23*, *24*). The YD basal boundary layer at Hall's Cave also contains purported ET proxies including nanodiamonds, aciniform soot, and magnetic spherules (*25*). Here, we present Os isotopes and HSE abundances from the YD basal boundary strata in addition to layers above and below that horizon. Our measurements span ~4000 years of sediment deposition at Hall's Cave. The HSE chondrite-normalized patterns combined with $^{187}Os/^{188}Os$ at different levels within this section at Hall's Cave including the YD basal boundary layer show a repeating record of Os concentration enrichment. Multiple occurrences above and below the anticipated YD basal boundary layer bring into question the single impact theory for the YD climate event. Instead, we propose that the five layers containing HSE enrichments and Os isotopic signatures represent volcanic aerosols and cryptotephra contributed from distant volcanic eruptions over the ~4000 years.

RESULTS

Osmium concentrations and $^{187}Os/^{188}Os$ ratios were measured on five bulk samples from the YD basal boundary dark layer, and 32 samples were measured from horizons above and below it in Hall's Cave (table S1). In total, samples were collected at high spatial and temporal resolution across depositional ages ranging from 9600 to 13,500 years B.P. (*25*). Hall's Cave bulk sediments display large variations in Os abundance from 22.6 to 4478 ppt and $^{187}Os/^{188}Os$ ratios from 0.12 to 2.35 (Fig. 1). The samples are divided into two groups based on their Os abundances and $^{187}Os/^{188}Os$ ratios. In the first group (n = 30, hereon named "radiogenic"), the samples have $^{187}Os/^{188}Os$ ratios from 1.11 to 2.35 and Os abundances from 22.6 to 56.9 ppt. This combination of high $^{187}Os/^{188}Os$ ratios and low 10's of ppt Os abundances is typical for continental crust sediments (*17*, *22*). The second group (n = 7, hereon "unradiogenic") has $^{187}Os/^{188}Os$ ratios from 0.12 to 0.42 and Os abundances from 105 to 4478 ppt. These values are not typical of continental crust and reflect an input from an ET or a mantle source. These samples come from five different horizons located at, above, and below the YD basal boundary layer (Fig. 1). Of the five YD basal boundary samples, four are radiogenic with $^{187}Os/^{188}Os$ values of 1.49 to 2.22, whereas only HC17_44 has a low, noncontinental crust-like $^{187}Os/^{188}Os$ value of 0.41 and Os abundance of 105 ppt.

Samples of Hall's Cave sediments with $^{187}Os/^{188}Os$ ratios of >1.11 (e.g., belonging to the radiogenic group) have CI chondrite–normalized HSE patterns that are indistinguishable from upper continental crust (Fig. 2). The unradiogenic samples, with $^{187}Os/^{188}Os$ ratios of ≤0.42, including the one sample in this group at the YDB layer, have low Ir, Ru, Pt, Pd, and Re abundances that are also similar to upper continental crust (Fig. 2 and table S1). Hence, there is no enrichment in these elements spanning across the YD section in Hall's Cave. This result is consistent with data from eight other YD locales (*21*). However, the CI chondrite–normalized HSE patterns for the unradiogenic

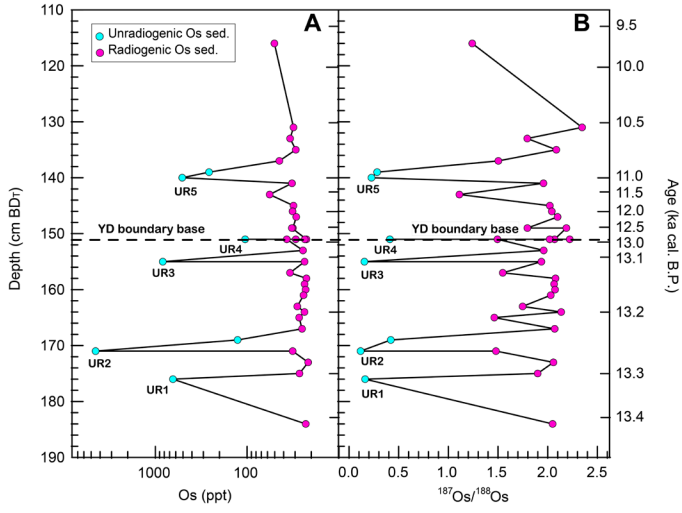

Fig. 1. Depth below datum (BD_T) profiles against total Os abundances (ppt) and $^{187}Os/^{188}Os$ ratios of Hall's Cave sample section. (**A**) Depth versus total Os abundances (ppt). (**B**) Depth versus $^{187}Os/^{188}Os$ ratios. Local datum used in this study was placed by Toomey, 1986 (*23*). UR, unradiogen. UR1 to UR5 represent five unradiogenic Os peaks. Depth values are the basal depth of the 1-cm-thick excavation interval relative to the datum. Six ages were calibrated using direct AMS ^{14}C measurements with 95.4% confidence intervals and then used to calculate the rest of the dates with linear interpolation between the dated levels.

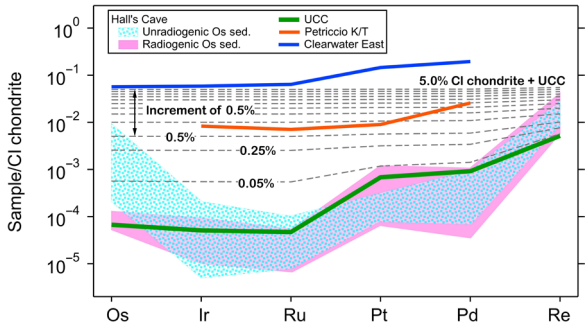

Fig. 2. CI chondrite–normalized incremental mixing model of CI chondrite material into an upper continental crust–like target. From 0.5 to 5.0% mixing lines use 0.5% increment, beneath are the 0.05 and 0.25% lines. HSE patterns of Hall's Cave unradiogenic Os sediments (blue dotted pattern) and radiogenic Os sediments (pink shadow) compared with average upper continental crust (UCC) (*18*, *26*), Clearwater East Impact melt rock, Canada (*51*), and Petriccio K/T boundary, Italy (*52*). CI chondrite values used for normalization are from Wasson and Kallemeyn (*27*).

$^{187}Os/^{188}Os$ samples display a distinct enrichment for Os concentrations relative to upper continental crust and the radiogenic samples (Fig. 2).

DISCUSSION

Testing the YD impact hypothesis using Os isotopes and HSE

The Os isotope systematics and HSE abundance patterns (Fig. 2) indicate that exotic materials were contributed during multiple time intervals to the continuous sedimentary record in Hall's Cave. It is unlikely that multiple impacts/airbursts at these distinct time intervals over ~4000 years had occurred (Fig. 1). Furthermore, a bolide compositional signature is unsupported with mass balance calculations for the $^{187}Os/^{188}Os$ ratios and HSE concentrations with end members of CI chondrite and upper continental crust. For Os, assuming CI chondrite values of $^{187}Os/^{188}Os = 0.127$ and Os of 486,000 ppt and upper continental crust values of $^{187}Os/^{188}Os = 1.3$ and Os of 30 ppt (*18*, *26*, *27*), the amount of meteorite material mixed into upper continental crust to explain the $^{187}Os/^{188}Os$ ratios of the Hall's Cave unradiogenic samples is 0.02 to 0.79%. Similar models using the other HSE indicate 0.05 to 5.00% contribution from a CI chondrite impactor. The addition of only 0.05% CI chondrite to the upper continental crust results in gentle positive slopes from Os to Re for CI chondrite–normalized patterns (Fig. 2). Increasing the amount of CI chondrite to 0.5 to 1.0%, to match the highest amounts of Os found in the unradiogenic samples, flattens the slopes of the mixtures. These models do not match the relative distribution or abundances observed in the unradiogenic samples with the Os-enriched concentrations (Fig. 2). The measured abundances are not matched by models using any other chondrite material, including enstatite, ordinary, or other carbonaceous chondrites (fig. S1 and table S3). Impact melts with purported admixed chondritic material show an even distribution of HSE (Fig. 2). No iron meteorite groups display the observed distinct enrichments in Os relative to Ir or the increasing abundances from Ru, to Pt, to Pd, and to Re relative to CI. Thus, mixing iron meteorites with upper continental crust will not result in the HSE patterns exhibited by the unradiogenic samples (fig. S1 and table S3).

The modeling above indicates that the combined HSE abundances and $^{187}Os/^{188}Os$ ratios are inconsistent with contribution from an ET impactor or bolide airburst in agreement with previous results from other YD locales (*21*). Failing a meteorite source, the source of the enrichments and isotopic signature remains unresolved. A better explanation must include a terrestrial source of material able to be supplied frequently and episodically across short time intervals (years to decades).

Volcanic origin of Hall's cave sediment $^{187}Os/^{188}Os$ and HSE variations

The Hall's Cave samples are characterized by a two end member mixing model based on $^{187}Os/^{188}Os$ ratios and 1/Os abundances (Fig. 3). Data from other YD locales with $^{187}Os/^{188}Os$ ratios scatter around the Hall's Cave data, consistent with distinct natural variations in the continental crust (fig. S1). Sediment cores from the Gulf of California and Cariaco Basin are not shown because Paquay *et al.* (*21*) have conclusively argued that their $^{187}Os/^{188}Os$ ratios reflect rehomogenization with seawater and, hence, lack evidence of an unradiogenic $^{187}Os/^{188}Os$ component added to the sediments. The bulk sediment, bulk spherules, residues, and leachates from the Melrose, PA YD locale (*22*) cluster around the unradiogenic $^{187}Os/^{188}Os$ samples from Hall's Cave. The leachates, which are surface films on the bulk spherules (*22*), plot to less radiogenic $^{187}Os/^{188}Os$ ratios and higher Os concentrations defined by the Hall's Cave samples. These relationships are consistent with mixing between Hall's Cave crust and components broadly similar to the unradiogenic $^{187}Os/^{188}Os$ spherule surface films. This hypothesized mixing can yield the variation in Os isotope systematics for Hall's Cave unradiogenic $^{187}Os/^{188}Os$ samples. This mixing from two HSE sources provides a possible causal link between these North American locales for the unradiogenic $^{187}Os/^{188}Os$ ratios, particularly for the Hall's Cave YD layer. The spherules deposited at the Melrose (PA) YD layer were interpreted to be airborne material (*22*). The unradiogenic surface films on the spherules are hypothesized to originate from a bolide as it ablated during heating in the Earth's atmosphere or as terrestrial material that was ejected back into the atmosphere and redeposited following impact. However, these scenarios are problematic. The $^{187}Os/^{188}Os$ ratios from 0.112 to 0.120 in the spherule surface films are unlike most meteorites that have $^{187}Os/^{188}Os$ ratios of $\geq$0.124, with a few from 0.120 to 0.124 and two at 0.117 (*22*). These low values in the spherule surface films are consistent with being ancient subcontinental mantle (SCM) of $\geq$2.4 billion years, but no known impact site of a YD age is present in areas where this material may be accessible (*22*). Thus, if the Os from these surface films are similar to the material within the YD layer in Hall's Cave, and potentially the other layers with unradiogenic $^{187}Os/^{188}Os$ ratios, then it is unlikely that this material came from a bolide, a series of bolides at different times, or from multiple impact sites. This conclusion is also in agreement with the HSE patterns of the Hall's Cave sediments that are inconsistent with being derived from a meteoritic source.

Instead, the unradiogenic $^{187}Os/^{188}Os$ ratios from 0.12 to 0.42 in seven of the Hall's Cave samples indicate that some type of mantle-derived material was likely incorporated into some sediment layers at different time intervals. The elevated Os concentrations in these samples of 105 to 4478 ppt relative to continental crust with 30 ppt Os, and the radiogenic $^{187}Os/^{188}Os$ samples with 22 to 55 ppt Os, are consistent with mantle-derived Os material being added to these layers. If it is not impact ejecta from ancient SCM as discounted by Wu *et al.* (*22*), then one possibility is that exposed ancient mantle peridotite or komatiite (1000 s of ppt Os) (*28*, *29*) with low $^{187}Os/^{188}Os$

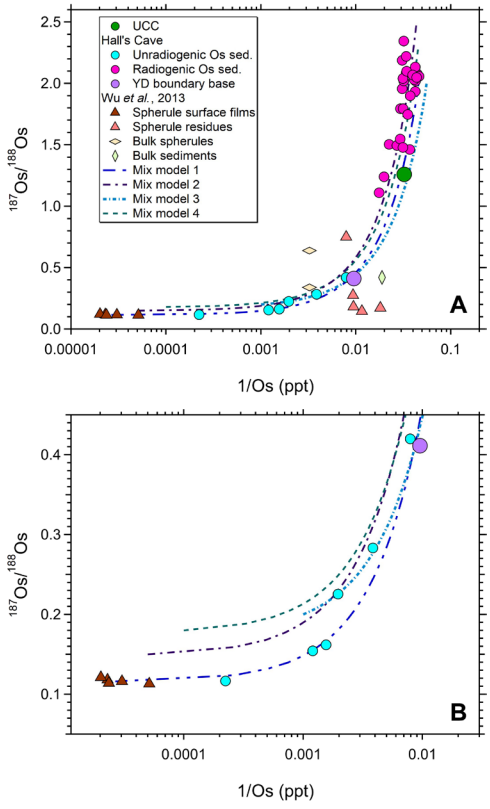

Fig. 3. Osmium isotope results and mixing models between Hall's Cave crusts and mantle-like Os end members. (**A**) $^{187}Os/^{188}Os$ versus 1/Os concentration (ppt) for Hall's Cave sediments with four mixing models for this study. Parameters used for the models are listed in table S4 (**B**) Mixing models close-up view on the lower left end of (A). Upper continental crust (*18*, *26*), data for bulk sediments, bulk spherules and spherule surface films, and residues were for the Melrose (PA) YD site from Wu *et al.* (*22*).

and high Os abundance was eroded and episodically provided a supply of sediment at these time intervals where the unradiogenic $^{187}Os/^{188}Os$ ratios are found in the layers. However, there are no known exposures of peridotite or komatiite within 100s km of Hall's Cave rendering this possibility unlikely. Another possibility is local mafic volcanic material with mantle-derived $^{187}Os/^{188}Os$ ratios that is subsequently eroded and deposited in Hall's Cave. Mafic volcanic material is also problematic from the perspective of not having a source of this material nearby to erode.

One final scenario is that the source of the unradiogenic $^{187}Os/^{188}Os$ may be airborne material from concurrent volcanic eruptions, which would alleviate the need for nearby older volcanic sources to erode and deposit material in Hall's Cave. If the unradiogenic $^{187}Os/^{188}Os$ ratios in the YD layer and, potentially, the other layers in Hall's Cave are of volcanic origin, then the very high abundances of Os in the Melrose surface films of ~19,000 to 43,000 ppt (*22*) could reflect aerosols enriched in HSE associated with airborne volcanic tephra from distant eruptions, which are enriched in Os with mantle-like $^{187}Os/^{188}Os$ ratios.

To test this hypothesis, we developed mixing models between Hall's Cave crust compositions and hypothetical mantle-like Os end members. These models were parameterized to examine the range of potential variation in these components when mixed together, simulating the unradiogenic $^{187}Os/^{188}Os$ and high Os concentrations in the Hall's Cave samples. Table S4 lists the Os concentrations and $^{187}Os/^{188}Os$ ratios for the end-member components used for the mixing calculations. In mix 1 (Fig. 3), the average of the leachates for objects 2, 4, 5, 11, and 13 from the Melrose locale was used as the unradiogenic $^{187}Os/^{188}Os$ end member. When this is mixed with Hall's Cave crust with 21 ppt Os and $^{187}Os/^{188}Os$ of 2.1, the mixing curve passes through the unradiogenic Os sample from the YD layer in Hall's Cave and three of the samples from the other layers in Hall's Cave. Three unradiogenic $^{187}Os/^{188}Os$ samples from other layers in Hall's Cave plot to higher values of $^{187}Os/^{188}Os$ and not along this mixing curve. Three other representative mixing curves are shown in Fig. 3, where the Hall's Cave crust end member varies from 18 to 23 ppt and $^{187}Os/^{188}Os$ ratios from 2.0 to 2.5, with the unradiogenic Os end member varying from as low as 1000 to approximately 40,000 ppt and $^{187}Os/^{188}Os$ ratios from 0.115 to 0.2. These mixing models are all hyperbolic, and all seven unradiogenic $^{187}Os/^{188}Os$ samples from Hall's Cave fall within the band of possible values generated by mixing this range of end-member compositions. This modeling indicates that the observed compositions of the Hall's Cave unradiogenic $^{187}Os/^{188}Os$ samples reflect a range in Os concentrations and $^{187}Os/^{188}Os$ values for unradiogenic Os end members when mixed with Hall's Cave crustal component. Thus, the different layers in Hall's Cave with unradiogenic $^{187}Os/^{188}Os$ ratios are unrelated to a single source of Os, as expected given the different depositional times but instead likely related to a process of high Os concentration material deposited having a range of $^{187}Os/^{188}Os$ values from around 0.115 to 0.20.

This range of $^{187}Os/^{188}Os$ values needed for the mantle end member are within the range present in volcanic lava samples worldwide, for example, the Cascade arc (0.129 to 0.253) (*30*), Ocean Island lavas from 0.110 to 0.176 (*31*), Ethiopian lavas from East African Rift (0.124 to 0.427) (*32*), and numerous other volcanic rock locales. Aerosols measured at Mauna Loa in Hawaii have $^{187}Os/^{188}Os$ ratios of 0.136 to 0.140 (*33*), consistent with the compositions of lavas from this volcano (*34*). Condensates from aerosols from Piton de la Fournaise fumarole on Reunion Island show that different sources can be tapped and that decoupling in the $^{187}Os/^{188}Os$ ratio can occur between lavas and aerosols (*35*). The samples from the lowest temperature condensates (<350°C) have $^{187}Os/^{188}Os$ ratios of 0.130 to 0.135 and overlapping those of the associated lavas. The highest temperature condensates (384 to 400°C) have $^{187}Os/^{188}Os$ ratios of 0.123 to 0.129, indicating derivation from older mantle sulfides and show that Os can be derived from different sources than those for the lavas resulting in distinct $^{187}Os/^{188}Os$ values. Hence, the lavas are not always a direct indication of the $^{187}Os/^{188}Os$ ratios for those of the associated aerosols, and these sources for Os can change during evolution of the volcano magmatic systems. What these relationships indicate is that if it is not unexpected, then that airborne cryptotephra with high Os concentration surface films derived from volcanic aerosols would have $^{187}Os/^{188}Os$ ratios consistent with the range of those needed to explain the range of unradiogenic $^{187}Os/^{188}Os$ sample values from Hall's Cave.

For this scenario, powerful volcanic eruptions provide the most likely source for the observed high Os abundances and low $^{187}Os/^{188}Os$ signatures at Hall's Cave and potentially explain the surface films on the Melrose spherules in the YD layer. The record of punctuated volcanism would be preserved as cryptotephra horizons with unique chemical fingerprints within the stratigraphy. Mafic melts contain

the highest concentrations of HSE with the concentration of at 0.1 to 1000 ppt (*31*, *36*). Fractional crystallization produces more silicic, evolved melts with lower HSE concentrations (e.g., Os of 10 to 34 ppt) (*36*, *37*). These values do not completely overlap with the Os concentrations preserved in the seven possible cryptotephra samples at Hall's Cave, which range from 105 to 4478 ppt. Volcanic degassing may provide the required mechanism that enriches low magmatic HSE concentrations to much higher values. During ascent and depressurization, volatiles exsolve from magma. Common volatiles include CO_2, H_2O, SO_2, H_2S, HCl, and HF. HSE partition strongly to an exsolved vapor phase, with estimated melt-vapor distribution coefficients as high as 10^5 to 10^6 (*38*, *39*). This process can be accentuated by both the increasing solubility of sulfur and increasing oxidation state of the magma during decompression. In oxidized magmas with lower amounts of H_2S, HSE concentrate in the melt where they are available to degas. This is because the sulfide minerals in which HSE would partition are unstable (*31*, *40*). Sulfur becomes increasingly soluble with decreasing pressure, which causes the melt to become sulfur undersaturated and forces HSE-bearing sulfides to dissolve back into the melt with subsequent gas release (*40*, *41*).

The HSE during an eruption is lost from the melt, added to the eruption column, exists in sulfur and other compounds, and adheres to ash particles (here, referred to as volcanic aerosols) (*35*, *38*). The magnitude of a volcanic eruption controls how high the plume penetrates the atmosphere, which subsequently controls the geographic distribution of the tephra. Large eruptions may thus entrain HSE far into the atmosphere where they can be transported long distances before deposition (*42*). Eruptions with magnitudes of >5 volcanic explosivity index (VEI) reach the stratosphere and can be globally distributed as volcanic aerosols (*43*). Volcanic aerosols have a significant impact on climate interactions, ozone chemistry, and vapor transport, and therefore, these particles have been the focus of observation and modeling (*40*). Particulate entrainment within the planetary wave train results in global distribution of volcanic aerosols from high-latitude volcanoes, with spread of the cryptotephra across the hemisphere, whereas equatorial eruptions may distribute volcanic aerosols in both hemispheres (*44*).

We contend from the analysis of Hall's Cave sediments that horizons with unradiogenic $^{187}Os/^{188}Os$ ratios are cryptotephra with surface films consisting of volcanic aerosols. Thus, the HSE concentrations should correspond to observed values in volcanic aerosols from eruptions in modern environments. The HSE values in Hall's Cave follow a trend showing a progressive increase in concentrations from Ru to Ir to Os and from Ru to Pt and Pd that closely matches the patterns of the Kudryavy volcano gas condensates, Kurile Islands (Fig. 4). In particular, Ir and Pt have been used to support the bolide hypothesis in other YD locales (*1*, *19*). As shown in Fig. 5, using Pt, Ir, Os, and Pd concentrations and ratios, the Hall's Cave unradiogenic Os samples instead closely match those for the range and variation of gas condensates from three different volcanoes (Fig. 5) (*36*, *38*, *41*). The range in HSE concentrations and ratios for all Hall's Cave samples plot as well-defined trends or clusters in these variation diagrams. These variations are consistent with the mixing scenario between volcanic aerosols with a range of HSE systematics related to specific supplies of material from different volcanoes, with upper continental crust, within any given unradiogenic $^{187}Os/^{188}Os$ layer, observed for $^{187}Os/^{188}Os$ versus 1/Os (Fig. 3) and that for $^{187}Os/^{188}Os$ versus Os/Ir (fig. S3).

The one HSE that is not showing a similar enrichment in the Hall's Cave unradiogenic $^{187}Os/^{188}Os$ samples to that expected from volcanic aerosol addition is Re. Rhenium, like Os, shows up to a two order of magnitude enrichment in volcanic aerosols relative to upper continental crust, but this is not observed in the Hall's Cave samples (Fig. 4). If the volcanic aerosol hypothesis is viable, then the question arises as to why there is no Re enrichment. There are two possible scenarios. In the first scenario, Re was redistributed in the sediments thereby erasing the aerosol signature. Rhenium can be highly mobile in the surface environment in oxidizing conditions where it can form ReO^{4-} (perrhenate). However, this is discounted because the Pt/Os and Re/Os ratios strongly correlate with $^{187}Os/^{188}Os$ in the Hall's Cave samples, indicating little to no HSE mobility (fig. S4).

In the second scenario, Re from volcanic aerosols is not condensing on cryptotephra surfaces that are transported long distances before deposition in locations such as Hall's Cave. The limited studies on volcanic systems to date indicate that the HSE can strongly fractionate from each other during volatile phase transport and condensation from the aerosols (*37*). The HSE fractionations and minerals condensed, such as rhenite (ReS_2), K-Re-perrhenate, and those for Pt-Pd and Os alloys, are dependent on the temperature of condensation and volatile compounds that are present in the aerosols (*38*). These can vary greatly from volcano to volcano as do the variations for HSE relative to each other in the aerosols (*38*, *39*, *45*). Further work will be required to better constrain the HSE relationships during these gaseous volcanic processes and as they relate to the observed aerosol fingerprints observed in the Hall's Cave unradiogenic $^{187}Os/^{188}Os$ samples and elsewhere.

Notably, the HSE systematics show only minor overlap with those for mafic and ultramafic lavas from different tectonic settings, further supporting a scenario where the HSE are fingerprinting the aerosols from volcanic systems and unlikely sourced from respective silicate magmas. In addition, impact-related materials have clearly different HSE systematics (Fig. 5), consistent with a non-ET source with low $^{187}Os/^{188}Os$ ratios for the unradiogenic samples. The HSE systematics in the Hall's Cave unradiogenic $^{187}Os/^{188}Os$ samples are thus best explained by input of cryptotephra with

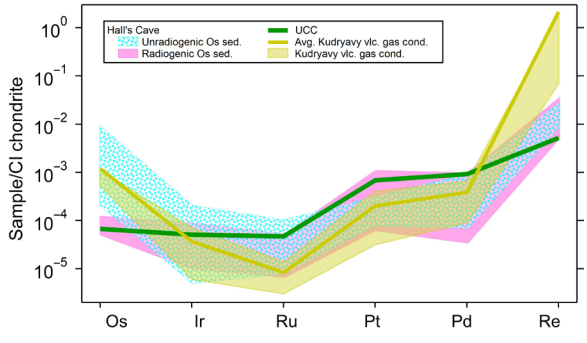

Fig. 4. CI chondrite–normalized HSE patterns of all gas condensates and the average of the Kudryavy volcano gas condensates, Kurile Islands. Upper continental crust is from Park *et al.* (*26*) and Esser and Turekian (*18*). The HSE patterns for the Os isotope radiogenic and unradiogenic groups from Hall's Cave are in pink shadow and blue dotted pattern, respectively. All Kudryavy volcano gas condensates (abbreviated to vlc. gas cond.) (*38*) are plotted as yellow shadow whose average is presented as the yellow line. CI chondrite values used for normalization are from Wasson and Kallemeyn (*27*).

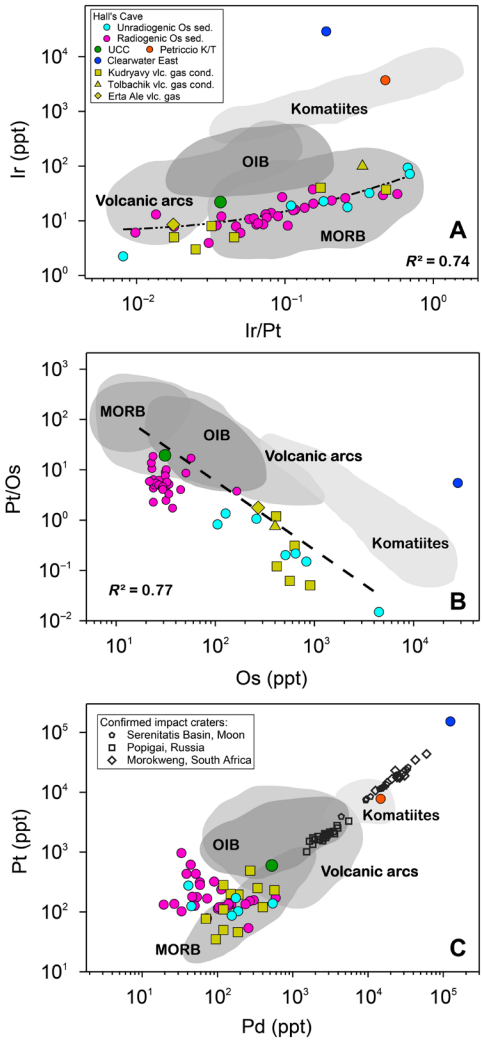

Fig. 5. Binary plots of HSE elements and ratios of Hall's Cave samples. (**A**) Ir versus Ir/Pt, (**B**) Pt/Os versus Os, (**C**) Pt versus Pd. compared to upper continental crust (*18*, *26*), Clearwater East Impact melt rock, Canada (*51*); Petriccio K/T boundary, Italy (*52*); Kudryavy volcano gas condensates, Kurile Islands (*38*); Tolbachik volcano gas condensate, Kamchatka (*45*); Erta Ale volcano gas (abbreviated to vlc. gas), Ethiopia (*39*) and confirmed impact craters, Popigai, Russia (*53*); Morokweng, South Africa (*16*); Serenitatis basin, Moon (*54*); MORB, mid-ocean ridge basalts (*55*, *56*); OIB, ocean island basalts (*57*, *58*); Volcanic arcs (*36*); and komatiites (*29*, *59*). (A) Ir versus Ir/Pt. (B) Pt/Os versus Os. (C) Pt versus Pd. See text for more information.

surfaces laden with HSE-enriched aerosols from distal, large-volume Plinian eruptions occurring at different times and added to the continental crust-derived sediments.

Timing of volcano eruptions with Hall's Cave sediment deposition

Distant volcanic eruptions may provide both the compositional control and physical mechanism to produce the HSE-enriched cryptotephra horizons in Hall's Cave. The multidecadal to century scale time resolution for sedimentation in Hall's Cave obviate correlation with specific volcanic eruptions. However, this section documents significant eruptions within the time frame of the cryptotephra horizons fingerprinted by $^{187}Os/^{188}Os$ ratios and HSE systematics. These times indicate active volcanism in regions in the Northern Hemisphere that could have contributed cryptotephra to Hall's Cave sediments. The cryptotephra horizon at 151 cm at the YD basal boundary layer at 13.11 to 12.90 ka was likely sourced from the 13.10 ± 0.10 ka eruption of Laacher See. The Laacher See eruption ejected 6.3 km^3 (DRE) of sulfur-rich magma far into the stratosphere and likely dispersed volcanic aerosols throughout the Northern Hemisphere (*8*, *9*). Laacher See released from 2 to 150 Mt of sulfur. Although under debate, this may have triggered the temperature decline associated with YD climate change in the Northern Hemisphere (*10*).

To identify possible volcanic sources for the other horizons in Hall's Cave that have $^{187}Os/^{188}Os$ ratios and HSE signatures consistent with cryptotephra, the ^{14}C ages of large-magnitude volcanic eruptions during the late Pleistocene to Holocene are compared to the ^{14}C ages of the five HSE-enriched unradiogenic horizons (UR1 to UR5) in Hall's Cave (Fig. 1 and table S5). The five interpreted cryptotephra horizons can be grouped into three volcanic mixing events that correlate well with known eruptions. The couplet of UR1 and UR2 horizons at 176 and 171 cm BD_T [below datum by Toomey in 1986; (*23*)], with a depositional age of 13.33 ± 0.19 ka, is similar to the Glacier Peak volcano in Washington, USA erupted at 13.71 to 13.41 ka and/or the J Swift tephra from Mount Saint Helens erupted at 13.75 to 13.45 ka (table S5). These eruptions demonstrate that the Cascade volcanic arc was highly active at these times and would likely have dispersed volcanic aerosols and cryptotephra widely across the Northern Hemisphere.

There are possibly two eruptive candidates for Horizon UR5 at 140 cm BD_T, which dates to 10.98 ka. Both the Fisher Tuff eruption from the Aleutian Arc and the Lvinaya Past eruption from the Kuril Arc occurred during the appropriate time interval (table S5). Each of these large-volume arc volcano eruptions produced a Plinian eruption column that reached the stratosphere and distributed volcanic aerosols across North America (*46*).

Significance of the Hall's cave HSE signatures and conclusions

The mass balance models using a range of chondrite and iron meteorite HSE abundances indicate that it is highly improbable that the addition of meteoritic impactor components into continental crust could reproduce the observed chondrite-normalized HSE patterns for the Hall's Cave unradiogenic $^{187}Os/^{188}Os$ samples. A two end member mixing relationship between Melrose (PA) spherule surface films and Hall's Cave bulk sediments demonstrate a distinctly different Os isotope systematics for the YD layer. The four other layers above and below the YD layer with unradiogenic $^{187}Os/^{188}Os$ ratios are consistent with mixing between Hall's Cave sediment and mantle-derived end members with a range of $^{187}Os/^{188}Os$ ratios from 0.115 to 0.2. This range of $^{187}Os/^{188}Os$ ratios overlaps those for lavas from different tectonic settings worldwide and those measured on volcanic aerosols. The HSE ratios and chondrite-normalized patterns for these samples from Hall's Cave display close similarity with volcanic aerosols. The five unradiogenic Os peaks, including the YD layer, fall within a ~4000-year time interval. The unradiogenic $^{187}Os/^{188}Os$ ratio and HSE abundance data from Hall's Cave sediments are inconsistent with the YD impact hypothesis. Alternatively, these levels contain cryptotephra and associated aerosols derived from large Plinian volcanic eruptions. The YD horizon correlates in time with the Laacher See eruption with a VEI of 6 and a 6.3-km^3 eruptive

volume that was dispersed throughout the Northern Hemisphere. Previously found YD markers, such as nanodiamonds and other wildfire products, are not necessarily solely impact-induced. Instead, these could originate from high-temperature, large-scale volcanic eruptions whose explosive conditions are capable of producing molten silica and carbon spherules and possibly nanodiamonds (Lonsdaleite) (*47*).

These observations from the Hall's Cave section also explain the lack of an Os isotope ET signature, or for the interpretation of a cryptotephra signature, at many YD locales across the Northern Hemisphere. Deposits of cryptotephra at any given time would be dependent on dispersal of the eruptive products from the volcanos emitting them, which could be localized or found in narrow bands depending on the dispersal patterns. This issue requires further investigation using HSE and Os isotopes to track dispersal dynamics.

The results here have implications for not only the YD event but also other Pt and Ir enrichment events in Earth history and where other supposed bolide markers have been used to support impacts at these times. This analysis indicates that coupled Os isotope and HSE concentration data are needed at close stratigraphic intervals above and below suspected bolide events to evaluate an alternative volcanic origin.

MATERIALS AND METHODS

Approximately 1-cm-thick sediment samples were taken consecutively along vertical sequences transecting the YDB layer in Hall's Cave. The depths are measured at the base of each 1-cm-thick sampling unit, for example, HC16_01 was extracted sediment between depths of 151 and 152 cm. Samples were dried at ~200°C for 3 hours. Hereafter, samples were weighed, spiked, and dissolved in reverse aqua regia using the Carius tube digestion method (*48*) at 240°C for a continuous ~48 hours. Subsequent acid solution processing was closely followed by CCl_4 solvent extraction (*49*), microdistillation (*50*), and ion exchange chromatography to obtain purified HSE and Os isotopes. Osmium isotope and HSE abundances were determined with a mixed spike via isotope dilution using a negative thermal ionization mass spectrometer Thermo Fisher Triton Plus and quadrupole inductively coupled plasma mass spectrometry (ICP-MS), respectively, at the University of Houston. No metal tools were used for collecting or transferring samples during any stage of the sampling or chemical processes. Details of sampling site, sampling techniques, HSE, and Os isotope methodology are given in the Supplementary Materials.

SUPPLEMENTARY MATERIALS

Supplementary material for this article is available at http://advances.sciencemag.org/cgi/content/full/6/31/eaax8587/DC1

REFERENCES AND NOTES

1. R. B. Firestone, A. West, J. P. Kennett, L. Becker, T. E. Bunch, Z. S. Revay, P. H. Schultz, T. Belgya, D. J. Kennett, J. M. Erlandson, O. J. Dickenson, A. C. Goodyear, R. S. Harris, G. A. Howard, J. B. Kloosterman, P. Lechler, P. A. Mayewski, J. Montgomery, R. Poreda, T. Darrah, S. S. Q. Hee, A. R. Smith, A. Stich, W. Topping, J. H. Wittke, W. S. Wolbach, Evidence for an extraterrestrial impact 12,900 years ago that contributed to the megafaunal extinctions and the Younger Dryas cooling. *Proc. Natl. Acad. Sci. U.S.A.* **104**, 16016–16021 (2007).
2. J. P. Severinghaus, T. Sowers, E. J. Brook, R. B. Alley, M. L. Bender, Timing of abrupt climate change at the end of the Younger Dryas interval from thermally fractionated gases in polar ice. *Nature* **391**, 141–146 (1998).
3. R. D. Guthrie, New carbon dates link climatic change with human colonization and Pleistocene extinctions. *Nature* **441**, 207–209 (2006).
4. L. Wang, W. Y. Jiang, D. B. Jiang, Y. F. Zou, Y. Y. Liu, E. L. Zhang, Q. Z. Hao, D. G. Zhang, D. T. Zhang, Z. Y. Peng, B. Xu, X. D. Yang, H. Y. Lu, Prolonged heavy snowfall during the Younger Dryas. *J. Geophys. Res. Atmos.* **123**, 13–748 (2018).
5. C. R. Moore, M. J. Brooks, A. C. Goodyear, T. A. Ferguson, A. G. Perrotti, S. Mitra, A. M. Listecki, B. C. King, D. J. Mallinson, C. S. Lane, J. D. Kapp, A. West, D. L. Carlson, W. S. Wolbach, T. R. Them, M. S. Harris, S. Pyne-O'Donnell, Sediment cores from white pond, south carolina, contain a platinum anomaly, pyrogenic carbon peak, and coprophilous spore decline at 12.8 ka. *Sci. Rep.* **9**, 15121 (2019).
6. K. H. Kjær, N. K. Larsen, T. Binder, A. A. Bjørk, O. Eisen, M. A. Fahnestock, S. Funder, A. A. Garde, H. Haack, V. Helm, M. Houmark-Nielsen, K. K. Kjeldsen, S. A. Khan, H. Machguth, I. McDonald, M. Morlighem, J. Mouginot, J. D. Paden, T. E. Waight, C. Weikusat, E. Willerslev, J. A. MacGregor, A large impact crater beneath Hiawatha Glacier in northwest Greenland. *Sci. Adv.* **4**, eaar8173 (2018).
7. G. R. Brakenridge, Core-collapse supernovae and the Younger Dryas/terminal Rancholabrean extinctions. *Icarus* **215**, 101–106 (2011).
8. E. Harms, H.-U. Schmincke, Volatile composition of the phonolitic Laacher See magma (12,900 yr BP): Implications for syn-eruptive degassing of S, F, Cl and H_2O. *Contrib. Mineral. Petrol.* **138**, 84–98 (2000).
9. H.-F. Graf, C. Timmreck, A general climate model simulation of the aerosol radiative effects of the Laacher See eruption (10,900 B.C.). *J. Geophys. Res. Atmos.* **106**, 14747–14756 (2001).
10. J. U. L. Baldini, R. J. Brown, N. Mawdsley, Evaluating the link between the sulfur-rich Laacher See volcanic eruption and the Younger Dryas climate anomaly. *Clim. Past.* **14**, 969–990 (2018).
11. J. H. Wittke, J. C. Weaver, T. E. Bunch, J. P. Kennett, D. J. Kennett, A. M. T. Moore, G. C. Hillman, K. B. Tankersley, A. C. Goodyear, C. R. Moore, I. R. Daniel, J. H. Ray, N. H. Lopinot, D. Ferraro, I. Israde-Alcántara, J. L. Bischoff, P. S. DeCarli, R. E. Hermes, J. B. Kloosterman, Z. Revay, G. A. Howard, D. R. Kimbel, G. Kletetschka, L. Nabelek, C. P. Lipo, S. Sakai, A. West, R. B. Firestone, Evidence for deposition of 10 million tonnes of impact spherules across four continents 12,800 y ago. *Proc. Natl. Acad. Sci. U.S.A.* **110**, E2088–E2097 (2013).
12. A. C. Scott, N. Pinter, M. E. Collinson, M. Hardiman, R. S. Anderson, A. P. R. Brain, S. Y. Smith, F. Marone, M. Stampanoni, Fungus, not comet or catastrophe, accounts for carbonaceous spherules in the Younger Dryas "impact layer". *Geophys. Res. Lett.* **37**, 10.1029/2010GL043345, (2010).
13. T. L. Daulton, S. Amari, A. C. Scott, M. Hardiman, N. Pinter, R. S. Anderson, Comprehensive analysis of nanodiamond evidence relating to the Younger Dryas impact hypothesis. *J. Quat. Sci.* **32**, 7–34 (2017).
14. T. A. Surovell, V. T. Holliday, J. A. M. Gingerich, C. Ketron, C. V. Haynes, I. Hilman, D. P. Wagner, E. Johnson, P. Claeys, An independent evaluation of the Younger Dryas extraterrestrial impact hypothesis. *Proc. Natl. Acad. Sci.* **106**, 18155–18158 (2009).
15. L. W. Alvarez, W. Alvarez, F. Asaro, H. V. Michel, Extraterrestrial cause for the Cretaceous-Tertiary extinction. *Science* **208**, 1095–1108 (1980).
16. I. McDonald, M. A. G. Andreoli, R. J. Hart, M. Tredoux, Platinum-group elements in the Morokweng impact structure, South Africa: Evidence for the impact of a large ordinary chondrite projectile at the Jurassic-Cretaceous boundary. *Geochim. Cosmochim. Acta* **65**, 299–309 (2001).
17. S. B. Shirey, R. J. Walker, The Re-Os isotope system in cosmochemistry and high-temperature geochemistry. *Annu. Rev. Earth Planet. Sci.* **26**, 423–500 (1998).
18. B. K. Esser, K. K. Turekian, The osmium isotopic composition of the continental crust. *Geochim. Cosmochim. Acta* **57**, 3093–3104 (1993).
19. M. I. Petaev, S. Huang, S. B. Jacobsen, A. Zindler, Large Pt anomaly in the Greenland ice core points to a cataclysm at the onset of Younger Dryas. *Proc. Natl. Acad. Sci. U.S.A.* **110**, 12917–12920 (2013).
20. C. R. Moore, A. West, M. A. LeCompte, M. J. Brooks, I. R. Daniel, A. C. Goodyear, T. A. Ferguson, A. H. Ivester, J. K. Feathers, J. P. Kennett, K. B. Tankersley, A. V. Adedeji, T. E. Bunch, Widespread platinum anomaly documented at the Younger Dryas onset in North American sedimentary sequences. *Sci. Rep.* **7**, 44031 (2017).
21. F. S. Paquay, S. Goderis, G. Ravizza, F. Vanhaeck, M. Boyd, T. A. Surovell, V. T. Holliday, C. V. Haynes, P. Claeys, Absence of geochemical evidence for an impact event at the Bølling–Allerød/Younger Dryas transition. *Proc. Natl. Acad. Sci.* **106**, 21505–21510 (2009).
22. Y. Wu, M. Sharma, M. A. LeCompte, M. N. Demitroff, J. D. Landis, Origin and provenance of spherules and magnetic grains at the Younger Dryas boundary. *Proc. Natl. Acad. Sci.* **110**, E3557–E3566 (2013).
23. R. S. Toomey, "Late Pleistocene And Holocene Faunal And Environmental Changes At Hall's Cave, Kerr County, Texas", thesis, The University of Texas at Austin (1993).
24. M. D. Bourne, J. M. Feinberg, T. W. Stafford, M. R. Waters, E. Lundelius, S. L. Forman, High-intensity geomagnetic field 'spike' observed at ca. 3000 cal BP in Texas, USA. *Earth Planet. Sci. Lett.* **442**, 80–92 (2016).

25. T. W. Stafford Jr., E. Lundelius, J. Kennett, D. J. Kennett, A. West, W. S. Wolbach, Testing Younger Dryas ET impact (YDB) evidence at Hall's Cave, Texas. *AGU Fall Meet. Abstr.* **33**, PP33B-08 (2009).
26. J.-W. Park, Z. Hu, S. Gao, I. H. Campbell, H. Gong, Platinum group element abundances in the upper continental crust revisited – New constraints from analyses of Chinese loess. *Geochim. Cosmochim. Acta* **93**, 63–76 (2012).
27. J. T. Wasson, G. W. Kallemeyn, Compositions of chondrites. *Phil Trans R Soc A Math. Phys. Eng. Sci.* **325**, 535–544 (1988).
28. A. D. Brandon, R. J. Walker, I. S. Puchtel, Platinum–osmium isotope evolution of the Earth's mantle: Constraints from chondrites and Os-rich alloys. *Geochim. Cosmochim. Acta* **70**, 2093–2103 (2006).
29. I. S. Puchtel, A. D. Brandon, M. Humayun, R. J. Walker, Evidence for the early differentiation of the core from Pt–Re–Os isotope systematics of 2.8-Ga komatiites. *Earth Planet. Sci. Lett.* **237**, 118–134 (2005).
30. L. E. Borg, A. D. Brandon, M. A. Clynne, R. J. Walker, Re–Os isotopic systematics of primitive lavas from the Lassen region of the Cascade arc, California. *Earth Planet. Sci. Lett.* **177**, 301–317 (2000).
31. J. M. D. Day, Hotspot volcanism and highly siderophile elements. *Chem. Geol.* **341**, 50–74 (2013).
32. W. R. Nelson, T. Furman, P. E. van Keken, S. B. Shirey, B. B. Hanan, Os–Hf isotopic insight into mantle plume dynamics beneath the East African Rift System. *Chem. Geol.* **320–321**, 66–79 (2012).
33. U. Krähenbühl, M. Geissbühler, F. Bühler, P. Eberhardt, D. L. Finnegan, Osmium isotopes in the aerosols of the mantle volcano Mauna Loa. *Earth Planet. Sci. Lett.* **110**, 95–98 (1992).
34. A. D. Brandon, M. D. Norman, R. J. Walker, J. W. Morgan, ^{186}Os–^{187}Os systematics of Hawaiian picrites. *Earth Planet. Sci. Lett.* **174**, 25–42 (1999).
35. A. Gannoun, I. Vlastélic, P. Schiano, Escape of unradiogenic osmium during sub-aerial lava degassing: Evidence from fumarolic deposits, Piton de la Fournaise, Réunion Island. *Geochim. Cosmochim. Acta.* **166**, 312–326 (2015).
36. S. J. Woodland, D. G. Pearson, M. F. Thirlwall, A platinum group element and Re–Os isotope investigation of siderophile element recycling in subduction zones: Comparison of Grenada, Lesser Antilles arc, and the Izu–Bonin arc. *J. Petrol.* **43**, 171–198 (2002).
37. J. C. Lassiter, J. F. Luhr, Osmium abundance and isotope variations in mafic Mexican volcanic rocks: Evidence for crustal contamination and constraints on the geochemical behavior of osmium during partial melting and fractional crystallization. *Geochem. Geophys. Geosystems.* **2**, 1027 (2001).
38. M. A. Yudovskaya, S. Tessalina, V. V. Distler, I. V. Chaplygin, A. V. Chugaev, Y. P. Dikov, Behavior of highly-siderophile elements during magma degassing: A case study at the Kudryavy volcano. *Chem. Geol.* **248**, 318–341 (2008).
39. M. E. Zelenski, T. P. Fischer, J. M. de Moor, B. Marty, L. Zimmermann, D. Ayalew, A. N. Nekrasov, V. K. Karandashev, Trace elements in the gas emissions from the Erta Ale volcano, Afar, Ethiopia. *Chem. Geol.* **357**, 95–116 (2013).
40. C. Oppenheimer, B. Scaillet, R. S. Martin, Sulfur degassing from volcanoes: source conditions, surveillance, plume chemistry and Earth system impacts. *Rev. Mineral. Geochem.* **73**, 363–421 (2011).
41. A. Gannoun, K. W. Burton, J. M. D. Day, J. Harvey, P. Schiano, I. Parkinson, Highly siderophile element and Os isotope systematics of volcanic rocks at divergent and convergent plate boundaries and in intraplate settings. *Rev. Mineral. Geochem.* **81**, 651–724 (2016).
42. R. W. Henley, B. R. Berger, Nature's refineries — Metals and metalloids in arc volcanoes. *Earth Sci. Rev.* **125**, 146–170 (2013).
43. A. Robock, Volcanic eruptions and climate. *Rev. Geophys.* **38**, 191–219 (2000).
44. C. Timmreck, H.-F. Graf, J. Feichter, Simulation of Mt. Pinatubo volcanic aerosol with the Hamburg climate model ECHAM4. *Theor. Appl. Climatol.* **62**, 85–108 (1999).
45. I. V. Chaplygin, V. Y. Lavrushin, E. O. Dubinina, Y. V. Bychkova, S. Inguaggiato, M. A. Yudovskaya, Geochemistry of volcanic gas at the 2012–13 New Tolbachik eruption, Kamchatka. *J. Volcanol. Geotherm. Res.* **323**, 186–193 (2016).
46. S. D. F. Pyne-O'Donnell, L. C. Cwynar, B. J. L. Jensen, J. H. Vincent, S. C. Kuehn, R. Spear, D. G. Froese, West Coast volcanic ashes provide a new continental-scale Lateglacial isochron. *Quat. Sci. Rev.* **142**, 16–25 (2016).
47. A. van Hoesel, W. Z. Hoek, G. M. Pennock, M. R. Drury, The Younger Dryas impact hypothesis: A critical review. *Quat. Sci. Rev.* **83**, 95–114 (2014).
48. S. B. Shirey, R. J. Walker, Carius tube digestion for low-blank rhenium-osmium analysis. *Anal. Chem.* **67**, 2136–2141 (1995).
49. A. S. Cohen, F. G. Waters, Separation of osmium from geological materials by solvent extraction for analysis by thermal ionisation mass spectrometry. *Anal. Chim. Acta* **332**, 269–275 (1996).
50. J. L. Birck, M. R. Barman, F. Capmas, Re-Os isotopic measurements at the femtomole level in natural samples. *Geostand. Newsl.* **21**, 19–27 (1997).
51. I. McDonald, Clearwater East impact structure: A re-interpretation of the projectile type using new platinum-group element data from meteorites. *Meteorit. Planet. Sci.* **37**, 459–464 (2002).
52. N. J. Evans, D. C. Gregoire, R. A. F. grieve, W. D. Goodfellow, J. veizer, Use of platinum-group elements for impactor identification: Terrestrial impact craters and Cretaceous-Tertiary boundary. *Geochim. Cosmochim. Acta.* **57**, 3737–3748 (1993).
53. R. Tagle, P. Claeys, An ordinary chondrite impactor for the Popigai crater, Siberia. *Geochim. Cosmochim. Acta.* **69**, 2877–2889 (2005).
54. R. Tagle, LL-Ordinary Chondrite Impact on the Moon: Results from the 3.9 Ga Impact Melt at the Landing Site of Apollo 17, in *36th Annual Lunar and Planetary Science Conference* (2005), vol. 36, p. 2008.
55. A. Bézos, J.-P. Lorand, E. Humler, M. Gros, Platinum-group element systematics in Mid-Oceanic Ridge basaltic glasses from the Pacific, Atlantic, and Indian Oceans. *Geochim. Cosmochim. Acta* **69**, 2613–2627 (2005).
56. A. Y. Yang, M.-F. Zhou, T.-P. Zhao, X.-G. Deng, L. Qi, J.-F. Xu, Chalcophile elemental compositions of MORBs from the ultraslow-spreading Southwest Indian Ridge and controls of lithospheric structure on S-saturated differentiation. *Chem. Geol.* **382**, 1–13 (2014).
57. T. J. Ireland, R. J. Walker, M. O. Garcia, Highly siderophile element and ^{187}Os isotope systematics of Hawaiian picrites: Implications for parental melt composition and source heterogeneity. *Chem. Geol.* **260**, 112–128 (2009).
58. J. M. D. Day, R. J. Walker, O. B. James, I. S. Puchtel, Osmium isotope and highly siderophile element systematics of the lunar crust. *Earth Planet. Sci. Lett.* **289**, 595–605 (2010).
59. B. D. Connolly, I. S. Puchtel, R. J. Walker, R. Arevalo Jr., P. M. Piccoli, G. Byerly, C. Robin-Popieul, N. Arndt, Highly siderophile element systematics of the 3.3Ga Weltevreden komatiites, South Africa: Implications for early Earth history. *Earth Planet. Sci. Lett.* **311**, 253–263 (2011).
60. E. H. Kastning, in *Multidisciplinary Conference on Sinkholes and the Environmental Impacts of Karst. 2* (1987), pp. 41–46.
61. C. I. Wong, J. L. Banner, M. Musgrove, Holocene climate variability in Texas, USA: An integration of existing paleoclimate data and modeling with a new, high-resolution speleothem record. *Quat. Sci. Rev.* **127**, 155–173 (2015).
62. A. Brauer, G. H. Haug, P. Dulski, D. M. Sigman, J. F. W. Negendank, An abrupt wind shift in western Europe at the onset of the Younger Dryas cold period. *Nat. Geosci.* **1**, 520–523 (2008).
63. C. Bronk Ramsey, Bayesian analysis of radiocarbon dates. *Radiocarbon* **51**, 337–360 (2009).
64. S. Goderis, A. D. Brandon, B. Mayer, M. Humayun, Osmium isotopic homogeneity in the CK carbonaceous chondrites. *Geochim. Cosmochim. Acta* **216**, 8–27 (2017).
65. J. M. D. Day, C. L. Waters, B. F. Schaefer, R. J. Walker, S. Turner, Use of hydrofluoric acid desilicification in the determination of highly siderophile element abundances and Re-Pt-Os isotope systematics in mafic-ultramafic rocks. *Geostand. Geoanalytical Res.* **40**, 49–65 (2016).
66. I. S. Puchtel, M. Humayun, Platinum group element fractionation in a komatiitic basalt lava lake. *Geochim. Cosmochim. Acta* **65**, 2979–2993 (2001).
67. M. Horan, R. J. Walker, J. W. Morgan, J. Grossman, A. Rubin, Highly siderophile elements in chondrites. *Chem. Geol.* **196**, 27–42 (2003).
68. J. M. D. Day, A. D. Brandon, R. J. Walker, Highly siderophile elements in Earth, Mars, the Moon, and asteroids. *Rev. Mineral. Geochem.* **81**, 161–238 (2016).
69. R. J. Walker, M. F. Horan, J. W. Morgan, H. Becker, J. N. Grossman, A. E. Rubin, Comparative ^{187}Re-^{187}Os systematics of chondrites: Implications regarding early solar system processes. *Geochim. Cosmochim. Acta* **66**, 4187–4201 (2002).
70. A. D. Brandon, M. Humayun, I. S. Puchtel, I. Leya, M. Zolensky, Osmium isotope evidence for an *s*-process carrier in primitive chondrites. *Science* **309**, 1233–1236 (2005).
71. M. Fischer-Gödde, H. Becker, F. Wombacher, Rhodium, gold and other highly siderophile element abundances in chondritic meteorites. *Geochim. Cosmochim. Acta* **74**, 356–379 (2010).
72. D. L. Cook, R. J. Walker, M. F. Horan, J. T. Wasson, J. W. Morgan, Pt-Re-Os systematics of group IIAB and IIIAB iron meteorites. *Geochim. Cosmochim. Acta* **68**, 1413–1431 (2004).
73. M. I. Petaev, S. B. Jacobsen, Differentiation of metal-rich meteoritic parent bodies: I. Measurements of PGEs, Re, Mo, W, and Au in meteoritic Fe-Ni metal. *Meteorit. Planet. Sci.* **39**, 1685–1697 (2004).
74. R. J. Walker, W. F. McDonough, J. Honesto, N. L. Chabot, T. J. McCoy, R. D. Ash, J. J. Bellucci, Modeling fractional crystallization of group IVB iron meteorites. *Geochim. Cosmochim. Acta* **72**, 2198–2216 (2008).
75. B. Peucker-Ehrenbrink, K. Hanghoj, T. Atwood, P. B. Kelemen, Rhenium-osmium isotope systematics and platinum group element concentrations in oceanic crust. *Geology* **40**, 199–202 (2012).
76. A. Gelinas, D. A. Kring, L. Zurcher, J. Urrutia-Fucugauchi, O. Morton, R. J. Walker, Osmium isotope constraints on the proportion of bolide component in Chicxulub impact melt rocks. *Meteorit. Planet. Sci.* **39**, 1003–1008 (2004).
77. J. T. Andrews, A. Geirsdóttir, J. Hardardóttir, S. Principato, K. Grönvold, G. B. Kristjansdóttir, G. Helgadóttir, J. Drexler, A. Sveinbjörnsdóttir, Distribution, sediment magnetism and geochemistry of the Saksunarvatn (10 180 ± 60 cal. yr BP) tephra in marine, lake, and terrestrial sediments, northwest Iceland. *J. Quat. Sci.* **17**, 731–745 (2002).

78. D. A. Neave, J. Maclennan, T. Thordarson, M. E. Hartley, The evolution and storage of primitive melts in the Eastern Volcanic Zone of Iceland: The 10 ka Grímsvötn tephra series (ie the Saksunarvatn ash). *Contrib. Mineral. Petrol.* **170**, 21 (2015).
79. R. Macdonald, B. Scaillet, The central Kenya peralkaline province: Insights into the evolution of peralkaline salic magmas. *Lithos* **91**, 59–73 (2006).
80. N. W. Rogers, P. J. Evans, S. Blake, S. C. Scott, C. J. Hawkesworth, Rates and timescales of fractional crystallization from ^{238}U–^{230}Th–^{226}Ra disequilibria in trachyte lavas from Longonot volcano, Kenya. *J. Petrol.* **45**, 1747–1776 (2004).
81. I. N. Bindeman, J. H. Fournelle, J. W. Valley, Low-δ^{18} O tephra from a compositionally zoned magma body: Fisher Caldera, Unimak Island, Aleutians. *J. Volcanol. Geotherm. Res.* **111**, 35–53 (2001).
82. P. Stelling, J. E. Gardner, J. Begét, Eruptive history of Fisher caldera, Alaska, USA. *J. Volcanol. Geotherm. Res.* **139**, 163–183 (2005).
83. N. G. Razzhigaeva, A. Matsumoto, M. Nakagawa, Age, source, and distribution of Holocene tephra in the southern Kurile Islands: Evaluation of Holocene eruptive activities in the southern Kurile arc. *Quat. Int.* **397**, 63–78 (2016).
84. S. Z. Smirnov, A. V. Rybin, E. N. Sokolova, D. V. Kuzmin, A. V. Degterev, T. Y. Timina, Felsic magmas of the caldera-forming eruptions on the Iturup Island: The first results of studies of melt inclusions in phenocrysts from pumices of the Lvinaya Past and Vetrovoy Isthmus calderas. *Russ. J. Pac. Geol.* **11**, 46–63 (2017).
85. A. Jennings, T. Thordarson, K. Zalzal, J. Stoner, C. Hayward, Á. Geirsdóttir, G. Miller, *Holocene Tephra from Iceland and Alaska in SE Greenland Shelf Sediments* (Geological Society, London, Special Publications, 2014), pp. 157–193.
86. E. L. Tomlinson, T. Thordarson, C. S. Lane, V. C. Smith, C. J. Manning, W. Müller, M. A. Menzies, Petrogenesis of the Sólheimar ignimbrite (Katla, Iceland): Implications for tephrostratigraphy. *Geochim. Cosmochim. Acta* **86**, 318–337 (2012).
87. Ø. S. Lohne, J. Mangerud, H. H. Birks, IntCal13 calibrated ages of the Vedde and Saksunarvatn ashes and the Younger Dryas boundaries from Kråkenes, western Norway. *J. Quat. Sci.* **29**, 506–507 (2014).
88. J. L. Arce, J. L. Macías, L. Vázquez-Selem, The 10.5 ka Plinian eruption of Nevado de Toluca volcano, Mexico: Stratigraphy and hazard implications. *Geol. Soc. Am. Bull.* **115**, 230–248 (2003).
89. C. B. Ramsey, P. G. Albert, S. P. E. Blockley, M. Hardiman, R. A. Housley, C. S. Lane, S. Lee, I. P. Matthews, V. C. Smith, J. J. Lowe, Improved age estimates for key Late Quaternary European tephra horizons in the RESET lattice. *Quat. Sci. Rev.* **118**, 18–32 (2015).
90. S. C. Kuehn, D. G. Froese, P. E. Carrara, F. F. Foit, N. J. Pearce, P. Rotheisler, Major-and trace-element characterization, expanded distribution, and a new chronology for the latest Pleistocene Glacier Peak tephras in western North America. *Quatern. Res.* **71**, 201–216 (2009).
91. J. E. Gardner, S. Carey, H. Sigurdsson, Plinian eruptions at Glacier Peak and Newberry volcanoes, United States: Implications for volcanic hazards in the Cascade Range. *Geol. Soc. Am. Bull.* **110**, 173–187 (1998).
92. L. I. Bazanova, I. V. Melekestsev, V. V. Ponomareva, O. V. Dirksen, V. G. Dirksen, Late Pleistocene and Holocene volcanic catastrophes in Kamchatka and in the Kuril Islands. Part 1. Types and classes of catastrophic eruptions as the leading components of volcanic catastrophism. *J. Volcanol. Seismol.* **10**, 151–169 (2016).
93. D. R. Mullineaux, "Pre-1980 tephra-fall deposits erupted from Mount St. Helens, Washington", in *Professional Paper* (USGS Numbered Series 1563, 1996); http://pubs.er.usgs.gov/publication/pp1563.
94. M. Shiihara, M. Torii, M. Okuno, H. Domitsu, T. Nakamura, K.-H. Kim, H. Moriwaki, M. Oda, Revised stratigraphy of Holocene tephras on Ulleung Island, South Korea, and possible correlatives for the U-Oki tephra. *Quat. Int.* **246**, 222–232 (2011).
95. G. B. Kim, S. J. Cronin, W. S. Yoon, Y. K. Sohn, Post 19 ka BP eruptive history of Ulleung Island, Korea, inferred from an intra-caldera pyroclastic sequence. *Bull. Volcanol.* **76**, 802 (2014).
96. A. L. Deino, G. Orsi, S. de Vita, M. Piochi, The age of the Neapolitan Yellow Tuff caldera-forming eruption (Campi Flegrei caldera–Italy) assessed by $^{40}Ar/^{39}Ar$ dating method. *J. Volcanol. Geotherm. Res.* **133**, 157–170 (2004).
97. R. Petrini, C. Forte, G. Contin, C. Pinzino, G. Orsi, Structure of volcanic glasses from the NMR-EPR perspective: A preliminary application to the Neapolitan Yellow Tuff. *Bull. Volcanol.* **60**, 425–431 (1999).

Acknowledgments: We thank Y. Gao (ICP Analytical Research Lab, University of Houston) for providing HSE standards and his assistance with quadrupole ICP-MS measurements at this facility. The experimental work could not have been accomplished without the help and support of A. Heri in the TIMS Lab at University of Houston. We thank T. W. Stafford for the calibrated ages using AMS ^{14}C measurements and his previous work at Hall's Cave obtaining precise radiocarbon ages laid the foundation for this study. The North Star Archaeological Research Fund and the Elfrieda Frank Foundation supported the field research at Hall's Cave. We thank the Hall family, especially Lee and Fran, for allowing us to work at the site and for all their hospitality. We also thank the three anonymous reviewers for their constructive comments, which substantially improved the quality of this paper. **Funding:** Os isotope and HSE concentration analyses costs were provided through the Geoluminescence Dating Research Laboratory at Baylor University, Waco, TX. The authors have no other funding to declare. **Author contributions:** N.S. measured the Os isotopic compositions and HSE abundances. N.S. and A.D.B. interpreted the data and drafted the initial manuscript. S.L.F., M.R.W., and N.S. conducted sample acquisition. All co-authors contributed, discussed, and edited the manuscript. **Competing interests:** The authors declare that they have no competing interests. **Data and materials availability:** All data needed to evaluate the conclusions in the paper are present in the paper and/or the Supplementary Materials. Additional data related to this paper may be requested from the authors.

Submitted 29 April 2019
Accepted 19 June 2020
Published 31 July 2020
10.1126/sciadv.aax8587

Citation: N. Sun, A. D. Brandon, S. L. Forman, M. R. Waters, K. S. Befus, Volcanic origin for Younger Dryas geochemical anomalies ca. 12,900 cal B.P. *Sci. Adv.* **6**, eaax8587 (2020).

Science Advances

Volcanic origin for Younger Dryas geochemical anomalies ca. 12,900 cal B.P.

N. Sun, A. D. Brandon, S. L. Forman, M. R. Waters and K. S. Befus

Sci Adv **6** (31), eaax8587.
DOI: 10.1126/sciadv.aax8587